

1 **Exploiting satellite measurements to explore uncertainties in**  
2 **UK bottom-up NO<sub>x</sub> emission estimates**

3  
4 Richard J. Pope<sup>1,2</sup>, Rebecca Kelly<sup>1</sup>, Eloise A. Marais<sup>3</sup>, Ailish M. Graham<sup>1</sup>,  
5 Chris Wilson<sup>1,2</sup>, Jeremy J. Harrison<sup>4,5</sup>, Savio J. A. Moniz<sup>6</sup>, Mohamed Ghalaieny<sup>6</sup>, Steve R.  
6 Arnold<sup>1</sup> and Martyn P. Chipperfield<sup>1,2</sup>  
7

8 *1: School of Earth and Environment, University of Leeds, Leeds, UK*

9 *2: National Centre for Earth Observation, University of Leeds, Leeds, UK*

10 *3: Department of Geography, University College London, London, UK*

11 *4: Department of Physics and Astronomy, University of Leicester, Leicester, UK*

12 *5: National Centre for Earth Observation, University of Leicester, Leicester, UK*

13 *6: Department for Environment, Food and Rural Affairs, 2 Marsham Street, London, UK*  
14  
15

16 Resubmitted to *Atmospheric Chemistry and Physics*

17 *Correspondence to:* Richard J. Pope (r.j.pope@leeds.ac.uk)

18 **Abstract**

19 Nitrogen oxides (NO<sub>x</sub>, NO+NO<sub>2</sub>) are potent air pollutants which directly impact on human  
20 health and which aid the formation of other hazardous pollutants such as ozone (O<sub>3</sub>) and  
21 particulate matter. In this study, we use satellite tropospheric column nitrogen dioxide  
22 (TCNO<sub>2</sub>) data to evaluate the spatiotemporal variability and magnitude of the United  
23 Kingdom (UK) bottom-up National Atmospheric Emissions Inventory (NAEI) NO<sub>x</sub> emissions.  
24 Although emissions and TCNO<sub>2</sub> represent different quantities, for UK city sources we find a  
25 spatial correlation of ~0.5 between the NAEI NO<sub>x</sub> emissions and TCNO<sub>2</sub> from the high-  
26 spatial-resolution TROPospheric Monitoring Instrument (TROPOMI), suggesting a good  
27 spatial distribution of emission sources in the inventory. Between 2005 and 2015, the NAEI  
28 total UK NO<sub>x</sub> emissions and long-term TCNO<sub>2</sub> record from the Ozone Monitoring Instrument  
29 (OMI), averaged over England, show annually decreasing trends of 4.4% and 2.2%,  
30 respectively. Top-down NO<sub>x</sub> emissions were derived in this study by applying a simple mass  
31 balance approach to TROPOMI observed downwind NO<sub>2</sub> plumes from city sources. Overall,  
32 these top-down estimates were consistent with the NAEI, but for larger cities such as  
33 London and [Manchester-Birmingham](#) the inventory is significantly (>25%) less than the top-  
34 down emissions.  
35  
36  
37  
38  
39

## 1. Introduction

Poor air quality (AQ) can have a substantial impact on human health, increasing risk of ailments such as asthma, cancer, diabetes and heart disease (Royal College of Physicians, 2016). A key air pollutant is nitrogen dioxide ( $\text{NO}_2$ ) which was responsible for approximately 9600 premature deaths from long-term exposure in the UK in 2015 (EEA, 2018).  $\text{NO}_2$  is also a precursor to tropospheric ozone and nitrate aerosol in the UK (DEFRA, 2018a). Legislation (e.g. the EU directive 2008/50/EC Ambient AQ regulation, (DEFRA, 2018a)) is in place to reduce concentrations of  $\text{NO}_2$  and other pollutants. However, many regions in the UK (33 out of 43 in 2019; DEFRA, 2020) still fail to meet the annual mean  $\text{NO}_2$  limit of  $40 \mu\text{g}/\text{m}^3$  (WHO, 2018). To meet the UK's statutory reporting requirements and to help inform policy, Defra uses the National Atmospheric Emissions Inventory (NAEI, 2021). However, like all emission inventories, the NAEI is subject to uncertainties which are difficult to quantify. These uncertainties include unreported sources, diffuse sources such as agriculture, the use of proxy data (e.g. population or housing density data) to distribute emissions and updates to the NAEI methodologies between years (NAEI, 2017). In addition, the NAEI only includes emissions from anthropogenic sources. Spatial verification of the NAEI AQ emissions, until recently (Tsagatakis et al., 2021), has been restricted to comparisons with surface sites, which have limited and disproportional spatial coverage. The NAEI is also used to drive regional models (e.g. the UK Met Office Air Quality in the Unified Model (AQUM, Savage et al., 2013) which provides the official national AQ forecasts), land use regression models (e.g. Wu et al., 2017) and Pollutant Climate Mapping (PCM) models (e.g. Dibbens and Clemens, 2015), where uncertainties in the emissions can then feed into the simulated AQ predictions and resultant public health advisories.

Satellite measurements of tropospheric column  $\text{NO}_2$  ( $\text{TCNO}_2$ ) have frequently been used to derive top-down emissions of nitrogen oxides ( $\text{NO}_x = \text{nitric oxide (NO)} + \text{NO}_2$ ), which can be used to evaluate bottom-up inventories. Some studies have used statistical fitting of observed downwind plumes of  $\text{TCNO}_2$  from anthropogenic sources (e.g. Beirle et al., 2011; Liu et al., 2016; Verstraeten et al., 2018), while others have used complex atmospheric chemistry models deploying approaches such as data assimilation (e.g. Miyazaki et al., 2016), mass balance (Martin et al., 2003) and model sensitivity experiments (e.g. Potts et al., 2021).

While model-derived estimates of  $\text{NO}_x$  emissions (e.g. from data assimilation) are robust, the methodology is computationally expensive and time intensive. Therefore, the statistical fitting to downwind plumes approach is a more achievable approach to derive top-down emissions, especially for government departments and agencies. Beirle et al. (2011) presented one of the first studies to use statistical fitting to downwind plumes for Riyadh, Saudi Arabia. The method was also applied to multiple megacities and compared with the bottom-up Environmental Database for Global Atmospheric Research (EDGAR) emission inventory (version 4.1). Verstraeten et al. (2018) used a similar, but modified, approach of a simple mass balance which assumes that the observed total mass of  $\text{NO}_2$  is a product of the emission rate and the effective lifetime. The assumption is that the removal of  $\text{NO}_2$  can be described by a first-order loss (i.e. the chemical decay of  $\text{NO}_2$  follows an exponential decay function with an e-folding time, and therefore distance from source).

In this study, we use satellite  $\text{TCNO}_2$  records to evaluate the spatial distribution and temporal evolution of the NAEI. In the past, and still presently, this is a challenge given the climatological meteorological conditions (i.e. frequent frontal systems with widespread

98 precipitation and cloud cover; Pena-Angulo et al., (2020)) experienced in the UK. Frequent  
99 cloud cover means that satellite instruments are severely restricted in their ability to  
100 retrieve information on trace gases and aerosols through the atmosphere (i.e. retrievals  
101 only between the top of atmosphere and cloud top). Therefore, the lack of robust  
102 observations makes it more difficult to clearly resolve large emission sources from space.  
103 Also, previous sensors (e.g. the Ozone Monitoring Instrument, OMI) have had relatively  
104 coarse horizontal spatial resolutions (in the order of 10-100 km) which are larger than most  
105 UK emissions sources. However, this work represents the first attempt to derive UK city-  
106 scale NO<sub>x</sub> emissions from the new state-of-the-art TROPOspheric Monitoring Instrument  
107 (TROPOMI), which has unparalleled spatial resolution in comparison to previous sensors  
108 (e.g. OMI). We apply a similar approach to Verstraeten et al. (2018), but determine the  
109 background NO<sub>2</sub> value and e-folding distance in different ways, to derive top-down NO<sub>x</sub>  
110 emission estimates of UK cities and thereby directly evaluate the NAEI estimates. Therefore,  
111 we can derive NO<sub>x</sub> emissions from previously undetectable sources (e.g. Manchester and  
112 Birmingham). From here on, we refer to this methodology as the simple mass balance  
113 approach (SMBA). The satellite observations used, NAEI and SMBA are described in Section  
114 2, the results presented in Section 3 and our conclusions discussed in Section 4.

115

## 116 **2. Data and Methods**

117

### 118 **2.1 NAEI Emissions**

119

120 The NAEI is the official UK bottom-up inventory of primary sources of emissions, used for  
121 statutory reporting, national air quality policy and driving regional air quality models (NAEI,  
122 2021). The contract to deliver the NAEI is led by a consortium managed by Ricardo Energy and  
123 Environment for the UK Department for Business, Energy and Industrial Strategy (BEIS) and  
124 the Department for Environment, Food and Rural Affairs (Defra). The NAEI is compiled on an  
125 annual basis according to internationally agreed methodologies (EMEP/EEA, 2019),  
126 encompassing sectors ranging from transport, industry, through to agriculture and domestic  
127 sources (Ricardo Energy and Environment, 2021). Here, we use the NAEI emissions from 2019,  
128 which is the most recent version publically available.

129

### 130 **2.2 Satellite Data**

131

132 OMI and TROPOMI are both nadir-viewing instruments on-board the NASA Aura and ESA  
133 Sentinel 5 – Precursor (S5P) polar orbiting satellites, respectively, and have local overpass  
134 times of 13:30. TROPOMI measures in the ultraviolet-visible (UV-Vis, 270-500 nm), similar to  
135 OMI (Boersma et al., 2007), as well as near-infrared (NIR, 675-775 nm) and short-wave  
136 infrared (SWIR, 2305-2385 nm) spectral ranges (Veefkind et al., 2012). TROPOMI and OMI  
137 have nadir pixel sizes of 3.5 km × 5.5 km (in the UV-Vis, 7.0 km × 7.0 km for other spectral  
138 ranges) and 13 km × 24 km, respectively. The OMI (DOMINO version 2 product) and TROPOMI  
139 (TM5-MP-DOMINO version 1.2/3x – OFFLINE product) data were downloaded from the  
140 Tropospheric Emissions Monitoring Internet Service (TEMIS) for January 2005 to December  
141 2015 and February 2018 to January 2020, respectively. Given the issues with large cloud cover  
142 in the UK, we use two years of TROPOMI TCNO<sub>2</sub> data to help increase the spatiotemporal  
143 sample size when deriving top-down emissions to evaluate the 2019 NAEI NO<sub>x</sub> emissions. The  
144 OMI row anomaly first occurred in 2008 (Torres et al., 2018) and over time has progressively

145 had a detrimental impact on retrieved TCNO<sub>2</sub>. The study by Pope et al., (2018) successfully  
 146 used the OMI record to look at long-term trends in UK TCNO<sub>2</sub>. However, after 2015, while still  
 147 retrieving robust signals over source regions, the row anomaly appears to be substantially  
 148 artificially enhancing background TCNO<sub>2</sub>. Therefore, as we consider regional trends in TCNO<sub>2</sub>  
 149 in Section 3.2, we did not use OMI TCNO<sub>2</sub> after 2015. The data has been processed using the  
 150 methodology of Pope et al., (2018) to map the TCNO<sub>2</sub> data onto a high-resolution spatial grid  
 151 (0.025° × 0.025°, ~2-3 km × ~2-3 km for TROPOMI, 0.05° × 0.05°, ~5 km × ~5 km for OMI). The  
 152 TROPOMI data were quality controlled for a cloud radiance fraction <0.5, a quality control flag  
 153 >0.75 and where the TCNO<sub>2</sub> value was > -1.0×10<sup>-5</sup> moles/m<sup>2</sup> (i.e. random values round 0.0  
 154 may be slightly negative or positive so we filter for TCNO<sub>2</sub> > -1.0×10<sup>-5</sup> moles/m<sup>2</sup> otherwise a  
 155 positive bias in average TCNO<sub>2</sub> is imposed). While TROPOMI provides the greatest spatial  
 156 resolution of any satellite instrument to measure air pollutants, suitable to derive TCNO<sub>2</sub>  
 157 emission estimates over UK city-scale sources, the retrieved TCNO<sub>2</sub> has been shown to have  
 158 a low bias. Over north-western Europe, Verhoelst et al., (2021) found that TROPOMI  
 159 underestimated TCNO<sub>2</sub> by approximately 20-30% when compared with surface TCNO<sub>2</sub>  
 160 measurements, which is consistent with Chan et al., (2020) and Dimitropoulou et al., (2020).  
 161 OMI data were processed for a geometric cloud fraction of <0.2, quality flag = 0 (which also  
 162 flags pixels influenced by the row anomaly (Braak, 2010)) and TCNO<sub>2</sub> > -1.0×10<sup>-5</sup> moles/m<sup>2</sup>.

### 163 2.3 Simplified Mass Balance Approach

164  
 165  
 166 To derive top-down emissions of NO<sub>2</sub> we use the SMBA, which is based on downwind plumes  
 167 of TROPOMI observed TCNO<sub>2</sub> from the target source where the observed total mass of NO<sub>2</sub>  
 168 (i.e. the source-related enhancement of TCNO<sub>2</sub> above the background level) is assumed to be  
 169 a product of the emission rate and the effective lifetime. Therefore, we can derive the  
 170 emission rate based on **Equation 1**:

$$171 \quad E = \frac{\sum_{i=0}^N ((NO_2 LD_i - B LD) \times \Delta d_i)}{t \times e^{-\frac{t}{\tau}}} \times f$$

$$172 \quad E = \frac{\sum_{i=0}^N (NO_2 LD_i \times \Delta d_i)}{t \times e^{-\frac{t}{\tau}}} \quad (1)$$

173 where  $E$  is the emission rate (moles/s),  $NO_2 LD$  is the  $NO_2$  line density (moles/m),  $B LD$  is the  
 174 background  $NO_2$  line density value (moles/m),  $\Delta d$  is the grid box length (m),  $i$  is the grid box  
 175 number between the source and background value,  $t$  is time (s) and  $e^{-\frac{t}{\tau}}$  is the e-folding loss  
 176 term with  $\tau$  as the effective lifetime.  $N$  represents the number of satellite TCNO<sub>2</sub> grid boxes  
 177 between the source and background level  $B$ .  $t$  is calculated as the distance between the  
 178 source and  $B$  divided by the wind speed ( $ws$ ). To derive the full  $NO_2$  loading emitted from the  
 179 source, the wind flow  $NO_2 LD$  has the background  $NO_2 LD$  (i.e.  $B LD$ ) value subtracted from all  
 180 points between the source and  $B$  and is then summed yielding the total  $NO_2$  mass (moles).  $f$   
 181 is the factor required to convert to  $NO_x$  emissions.  
 182 where  $E$  is the emission rate (moles/s),  $NO_2$   
 183  $LD$  is the  $NO_2$  line density (moles/m),  $\Delta d$  is the grid box length (m),  $i$  is the grid box number  
 184 between the source and background value,  $t$  is time (s) and  $e^{-\frac{t}{\tau}}$  is the e-folding loss term with  
 185  $\tau$  as the effective lifetime.  $N$  represents the number of satellite TCNO<sub>2</sub> grid boxes between the  
 186 source and background level  $B$ .  $t$  is calculated as the distance between the source and  $B$   
 187 divided by the wind speed ( $ws$ ). To derive the full  $NO_2$  loading emitted from the source, the

187 ~~wind flow  $NO_2$  LD has the background  $NO_2$  LD value subtracted from all points between the~~  
188 ~~source and  $B$  and is then summed yielding the total  $NO_2$  mass (moles).~~

189  
190 The wind speed and direction at a particular source are determined from the European Centre  
191 for Medium-Range Weather Forecasts (ECMWF, 2021) ERA5 u- & v-wind component data.  
192 The wind data are sampled at 13:00 UTC (around 13:00 local time (LT) over the UK) to coincide  
193 with the TROPOMI overpass (i.e. 13:30 LT) and averaged across boundary layer pressure levels  
194 (i.e. surface to 900 hPa). In all cases, the  $w_s$  had to be greater than 2 m/s to avoid near stable  
195 meteorological conditions. [Wind data is only used on days where there is TROPOMI  \$NO\_2\$  data](#)  
196 [available downwind of the target source, when deriving the average directional wind speed.](#)  
197 Studies such as Beirle et al. (2011) and Verstraeten et al. (2018) averaged the wind speeds  
198 over the surface to 500 m layer. Beirle et al. (2011) suggested that the average winds across  
199 this altitude range yielded uncertainties over approximately 30%, but neither study provided  
200 definitive reasoning why 500 m was selected. In the UK, 500 m is approximately 950 hPa which  
201 sits comfortably within the boundary layer (approximately 1000 m or 880.0 to 910 hPa in  
202 **Figure 1a** based on ERA-5 data sampled at 13.00 LT and averaged for 2019). In this study, we  
203 argue that wind speeds throughout the boundary layer are likely to be important in  
204 controlling the spatial distribution of  $NO_2$  downwind of sources. **Figure 1b** shows the zonally  
205 averaged latitude-pressure  $NO_2$  profile from the Copernicus Atmosphere Monitoring Service  
206 (CAMS, 2021), sampled at 13.00 LT and averaged for 2019, over the UK. The bulk of the  $NO_2$   
207 loading is near the surface with  $NO_2$  concentrations of 0.5 ppbv to >1.0 ppbv between the  
208 surface and 900 hPa. As shown by the white dashed lines, 60-70% of the surface to 500 hPa  
209  $NO_2$  loading exists between the surface and 900 hPa. The zonally averaged boundary layer  
210 pressure (red dashed line) also straddles the 900 hPa level. In **Figure 1c**, the wind speed profile  
211 for London sampled under westerly flow increases with altitude until between 925 hPa and  
212 900 hPa. For each pressure level, London westerly days are defined based average u- and v-  
213 components between the surface and the respective pressure level. As shown by the blue  
214 text, the wind speed gradient with respect to pressure substantially decreases (i.e. from -  
215 0.0406 m/s/hPa between 950 hPa and 925 hPa to -0.0045 m/s/hPa between 925 hPa and 900  
216 hPa) at 900 hPa. Therefore, this profile gradient and the information in **Figures 1a & b** suggest  
217 that 900 hPa is a suitable level to derive the boundary layer average wind speed and flow  
218 direction. The table (**panel d**) in **Figure 1** shows the sensitivity of the  $NO_x$  emission parameters  
219 to the pressure layer used. The derivation of emissions is discussed further in this section. The  
220 surface-850 hPa average and surface only winds show substantially different  $NO_x$  emission  
221 rates of 61.6 moles/s and 30.1 moles/s, respectively. However, the intermediate levels (900  
222 hPa and 950 hPa) show less dramatic step changes with emission rates of 55.2 moles/s and  
223 49.8 moles/s. Therefore, the surface-900 hPa layer is used to help derive  $NO_x$  emission rates  
224 in this study.

225  
226 The  $NO_2$  LD is the product of the source width, which is perpendicular to the wind flow, and  
227 the source-width-average  $TCNO_2$  (i.e. for each downwind grid box from the source, the  
228 [corresponding perpendicular rows between the source edges are averaged together](#)) profile  
229 downwind from the source on a grid box by grid box basis as shown in **Equation 2**.

$$NO_2LD_{i=1,N} = \frac{\sum_{j=1}^n TCNO_{2i,j}}{n} \times w \quad (2)$$

233 where  $NO_2 LD$  (moles/m) is the  $NO_2$  line density,  $i$  the grid box index downwind of the source  
234 starting at  $i=1$  going to  $i=N$  at background point  $B$ ,  $TCNO_2$  is the tropospheric column  $NO_2$  grid  
235 box value (moles/m<sup>2</sup>) at point  $i$  and  $j$  is the grid box index for the number of grid boxes  $n$ ,  
236 perpendicular to the downwind profile, which fit across the width of the source at grid box  $i$   
237 downwind and  $w$  is the source width (m) (i.e. source width perpendicular to the downwind  
238 profile) of the  $NO_2$  source. ~~Though the source width and length are subjective choices~~  
239 ~~the source width is a subjective choice~~ between the source edge locations, the same source  
240 width ~~and length values are used~~ ~~value is used~~ when deriving the TROPOMI  $NO_x$  emissions  
241 and summing up the NAEI  $NO_x$  emissions over the source region. As the source emissions will  
242 be a function of the source width (i.e. larger at source centre and lower at source edge), the  
243 mean  $TCNO_2$  downwind profile is representative of the source-average  $NO_2$  emission.

244  
245 **Figure 2a** shows the difference between TROPOMI  $TCNO_2$  sampled under westerly flow and  
246 the long-term average based on London u- and v-wind components, where there are clear  
247 downwind positive anomalies  $>3.0 \times 10^{-5}$  moles/m<sup>2</sup>. Similarly in **Figure 2b**, the downwind  
248 plume (e.g. westerly flow over London) has typically larger  $NO_2 LD$  values than the all-flow  
249 (i.e. all wind directions)  $NO_2 LD$ . The full  $NO_2$  mass emitted from the source in the  $NO_2 LD$  is  
250 the summation of the wind-flow  $NO_2 LD$  from source up to point  $B$  minus the background  
251 value from all downwind pixels over this profile segment. A reasonable estimate of when the  
252 wind-flow  $NO_2 LD$  reaches  $B$ , for more isolated  $NO_2$  sources, is when it intersects with the all-  
253 flow  $NO_2 LD$  profile (i.e. returns to normal levels). However, when there are substantial  
254 upwind  $NO_2$  sources, this can yield wind-flow  $NO_2 LD$  profiles which never intersect with the  
255 all-flow  $NO_2 LD$  profile within the domain (e.g. see Birmingham example in **Figure 3a & b**).  
256 ~~Therefore, to determine when  $B$ , in the downwind direction, has been reached, a running t-~~  
257 ~~test was applied to the wind-flow  $NO_2 LD$  profile to determine where turning points or~~  
258 ~~levelling off occurred. Such a substantial change in the  $NO_2 LD$  profile gradient is indicative of~~  
259 ~~the background level being reached and potentially another source being identified (e.g. in~~  
260 ~~**Figure 2b** there is evidence of other  $NO_2$  sources downwind of London several hundred~~  
261 ~~kilometres away over continental Europe). As such a test can be sensitive to noise in the~~  
262  ~~$TCNO_2$  data, a 10-pixel ( $0.5^\circ$ ) running average wind-flow  $NO_2 LD$  profile was calculated. This~~  
263 ~~smoothed out the noise from the downwind profile and allowed for the detection of larger-~~  
264 ~~scale  $NO_2 LD$  changes. The running t-test was applied to this using two windows (i.e. a moving~~  
265 ~~centre point with a window each side of  $0.5^\circ$ ) and the t-test significance between the two~~  
266 ~~window averages determined. This yielded a t-test significance/p-value distance series from~~  
267 ~~the source. When a substantial change in the  $NO_2 LD$  gradient occurred, the t-test p-values~~  
268 ~~would increase, peak and then drop off. This change in the gradient of the t-test p-~~  
269 ~~values identified the location of any  $NO_2 LD$  step changes in the profile. The green line in~~  
270 ~~**Figure 2b** shows where the t-test p-values peaked and that there are turning points in the~~  
271 ~~wind-flow  $NO_2 LD$  profile. Such a reduction in the wind-flow  $NO_2 LD$  profile gradient is~~  
272 ~~suggestive of the plume reaching  $B$  as  $NO_2$  levels have stabilised. However, in **Figure 2b**, there~~  
273 ~~are multiple locations potentially meeting this criteria. In reality, the turning points further~~  
274 ~~downwind of London are sources from the Benelux region. The red dot represents the first~~  
275 ~~instance, after the initial near-source wind-flow  $NO_2 LD$  peak, where the gradient in the~~  
276 ~~running t-test p-value profile changes sign (i.e. positive to negative or vice versa).~~

277  
278 ~~Therefore, to determine when  $B$  has been reached, a running t-test was applied to the wind-~~  
279 ~~flow  $NO_2 LD$  profile to determine where turning points or levelling off occurred. As such a test~~

280 can be sensitive to noise in the TCNO<sub>2</sub> data, a 10-pixel (0.5°) running average wind-flow NO<sub>2</sub>  
281 LD profile was calculated. The running t-test was applied to this using two windows of the  
282 same size to identify step-changes in the profile. The green line in **Figure 2b** shows where the  
283 t-test p-value has become large and there is a turning point in the wind-flow NO<sub>2</sub>-LD profile.  
284 Such a reduction in the wind-flow NO<sub>2</sub>-LD profile gradient is suggestive of the plume reaching  
285 *B* as NO<sub>2</sub> levels have stabilised. However, in **Figure 2b**, there are multiple locations potentially  
286 meeting this criteria. In reality, the turning points further downwind of London are sources  
287 from the Benelux region. The red dot represents the first instance, after the initial near-source  
288 wind-flow NO<sub>2</sub>-LD peak, where the gradient in the running t-test p-value profile changes sign  
289 (i.e. positive to negative or vice versa).

290 The loss term  $e^{-\frac{t}{\tau}}$  is dependent upon  $\tau$  and is determined by applying an e-folding distance fit  
291 between the near-source peak wind-flow NO<sub>2</sub> LD value and *B* (i.e. we assume this function is  
292 valid only between these two points), before dividing by *ws* to get  $\tau$ . Here, a range of e-folding  
293 distances are tested in the loss term  $e^{-\frac{t}{\tau}}$  to find the distance value which yields the lowest  
294 root mean square error (RMSE), and a large R<sup>2</sup> (Pearson correlation coefficient squared) value,  
295 between the e-folding distance fit (red line, **Figure 2c**) and the wind-flow NO<sub>2</sub> LD (black line,  
296 **Figure 2c**). In the case of London, this yielded an e-folding distance of 148.0 km and  $\tau$  of 4.5  
297 hours (8.64.7 and 4.33.1 hours) based on the average *ws* = 9.1 m/s with an uncertainty range  
298 ( $\pm$  04.34 m/s; i.e.  $\pm$  1-sigma standard deviation error) of 84.78 m/s to 139.5.4 m/s (i.e. a  
299 slower/faster wind speed yields a longer/shorter lifetime). The effective lifetime derived here  
300 for London and other UK cities is typically consistent with values from other studies (e.g. Beirle  
301 et al., (2011) and Verstraeten et al. (2018)) for European cities (i.e. 1.0 –10.0 hours).

302  
303 The top-down *E* is calculated from Equation 1 and this emissions flux of NO<sub>2</sub> (moles/s) is  
304 converted to emissions of NO<sub>x</sub> (moles/s) using the factor *f* for comparison with the bottom-  
305 up inventories. This is done by scaling the NO<sub>2</sub> emissions by 1.32 based on the NO:NO<sub>2</sub>  
306 concentration ratio (0.32) in urban environments at midday (Seinfeld and Pandis, 2006; Liu et  
307 al., 2016).~~The top-down *E* is calculated from Equation 1, but this is an emissions flux of NO<sub>2</sub>~~  
308 ~~moles/s which needs to be converted to NO<sub>x</sub> for comparison with the bottom-up inventories.~~  
309 ~~This is done by scaling the NO<sub>2</sub>-emissions by 1.32 based on the NO:NO<sub>2</sub>-concentration ratio~~  
310 ~~(0.32) in urban environments at midday (Seinfeld and Pandis, 2006; Liu et al., 2016).~~  
311 Verstraeten et al., (2018) used modelled NO and NO<sub>2</sub> concentrations to derive a scaling more  
312 representative of the chemistry of the source. They estimate there is a 10% uncertainty  
313 (similar to Beirle et al., (2011)), but as the modelled NO<sub>2</sub>:NO<sub>x</sub> ratio is based on the input  
314 emissions, for which the satellite data is being used to evaluate, this process is rather circular  
315 and not independent. ~~The final emission uncertainty estimates (Figure 2) are derived by  $\pm$  the~~  
316 ~~satellite error (10<sup>-5</sup> moles/m<sup>2</sup>) before obtaining the NO<sub>2</sub>-LD (Sat NO<sub>x</sub> Emissions 1) and by using~~  
317 ~~the uncertainties in  $\tau$  when determining the loss term (Sat NO<sub>x</sub> Emissions 2).~~

318  
319 Here, the top-down NO<sub>x</sub> emissions are derived by sampling TCNO<sub>2</sub> data under different wind  
320 directions in all seasons. Several studies, such as Beirle et al. (2011), have gone a step further  
321 and used TCNO<sub>2</sub> data to derive seasonal emissions. Unfortunately, here we are restricted to  
322 looking at annually derived emissions due to 1) the TROPOMI TCNO<sub>2</sub> record only started in  
323 February 2018, 2) the COVID-19 pandemic resulted in a dramatic reduction in UK (and global)  
324 NO<sub>x</sub> emissions (Potts et al., 2021) meaning TCNO<sub>2</sub> data beyond February 2020 could not be  
325 used to derive top-down emissions under normal conditions and 3) the UK is subject to

326 frequently cloudy conditions yielding a reduction in the number of observations from  
 327 TROPOMI. The latter point predominantly influences TROPOMI retrievals in the winter-time.  
 328 Therefore, even though we sample TCNO<sub>2</sub> data in all seasons, there is likely to be a tendency  
 329 towards summer-time TCNO<sub>2</sub> values, when TCNO<sub>2</sub> values tend to be lower (e.g. Pope et al.,  
 330 2015), potentially leading to a low bias in the derived top-down NO<sub>x</sub> emissions.

331 To investigate the total errors in the derived NO<sub>x</sub> emissions from TROPOMI, we have  
 332 included errors from all the input terms. These include the enhancement in the TCNO<sub>2</sub> data,  
 333 the e-folding distance  $x_0$ , the wind speed  $ws$ , the source width  $w$ , the NO<sub>2</sub> to NO<sub>x</sub> conversion  
 334 factor  $f$  and the distance  $d$  between the source and  $B$ . When combined, this yields the total  
 335 error in Equation 3:

$$336 \quad \Delta E = E \sqrt{\frac{\Delta\phi^2}{\phi^2} + \frac{\Delta ws^2}{ws^2} + \frac{\Delta w^2}{w^2} + \frac{\Delta f^2}{f^2} + \frac{d^2}{x_0^2} \left[ \frac{\Delta d^2}{d^2} + \frac{\Delta x_0^2}{x_0^2} \right]} \quad (3)$$

337 In the total error expression, we have set  $\phi = \overline{NO_2} - B$ , where  $\overline{NO_2}$  is the average TCNO<sub>2</sub>  
 338 value (moles/m<sup>2</sup>) for all grid cells between the source and  $B$  (i.e. background TCNO<sub>2</sub> value) in  
 339 the downwind profile. Here, we take  $\phi \times d \times w$  to be a suitable estimate of the full NO<sub>2</sub>  
 340 emission loading from the source (i.e. the numerator of Equation 1). Regarding the errors  
 341 (i.e. terms with  $\Delta$  in front), based on Beirle et al., (2011), we assign errors of 10% to  $f$  and  $w$ .  
 342 As  $x_0$  and  $d$  are distance metrics as well, with no clear way to quantify the errors in these  
 343 terms, we have assigned them with 10% errors also. The  $ws$  error is based on the standard  
 344 error in the sample (i.e. the number days selected for each flow regime). For the  
 345 enhancement in TCNO<sub>2</sub> from the source (i.e.  $\phi$ ), we have conservatively taken the largest  
 346 precision error value from all TCNO<sub>2</sub> values between the source and  $B$ , which forms  $\overline{NO_2}$ .

347

348

### 349 **3. Results**

350

#### 351 **3.1 NO<sub>x</sub> Sources**

352

353 Surface emissions and observed TCNO<sub>2</sub> represent different quantities and are influenced by  
 354 different processes. However, the short NO<sub>2</sub> lifetime of a few hours (Schaub et al., 2007; Pope  
 355 et al., 2015) means there is a sharp gradient between sources and the background levels.  
 356 Therefore, we can use the satellite TCNO<sub>2</sub> observations to provide some constraint on the  
 357 spatial distribution of the NO<sub>x</sub> emissions. In **Figure 4**, spatial maps over south-eastern (**Figure**  
 358 **4a & c**) and northern England (**Figure 4b & d**) show evidence of co-located TCNO<sub>2</sub> and NO<sub>x</sub>  
 359 emission hot spots, especially over many of the UK cities shown by circles. Here, both data  
 360 sets have been mapped onto the spatial resolution of 0.025° × 0.025°. In South East England,  
 361 TCNO<sub>2</sub> and NO<sub>x</sub> emissions peak over London at over 14.0 × 10<sup>-5</sup> moles/m<sup>2</sup> and approximately  
 362 >2.0 µg/m<sup>2</sup>/s, respectively. A secondary peak is also observed over western London for both  
 363 quantities at similar levels. There are further co-located hotspots over Southampton (TCNO<sub>2</sub>  
 364 ~8.0-9.0 × 10<sup>-5</sup> moles/m<sup>2</sup>, NO<sub>x</sub> >2.0 µg/m<sup>2</sup>/s), Portsmouth (TCNO<sub>2</sub> ~6.0-7.0 × 10<sup>-5</sup> moles/m<sup>2</sup>, NO<sub>x</sub>  
 365 ~1.0-1.5 µg/m<sup>2</sup>/s), Brighton (TCNO<sub>2</sub> ~5.0-6.0 × 10<sup>-5</sup> moles/m<sup>2</sup>, NO<sub>x</sub> ~0.5-0.8 µg/m<sup>2</sup>/s), Oxford  
 366 (TCNO<sub>2</sub> ~7.0-7.5 × 10<sup>-5</sup> moles/m<sup>2</sup>, NO<sub>x</sub> ~0.7-1.0 µg/m<sup>2</sup>/s) and Chelmsford (TCNO<sub>2</sub> ~8.5-9.5 × 10<sup>-5</sup>  
 367 moles/m<sup>2</sup>, NO<sub>x</sub> ~0.5 µg/m<sup>2</sup>/s). In northern England and the Midlands, peak TCNO<sub>2</sub> and NO<sub>x</sub>  
 368 emissions are located over Manchester (TCNO<sub>2</sub> ~10.0-11.0 × 10<sup>-5</sup> moles/m<sup>2</sup>, NO<sub>x</sub> ~1.0-1.5  
 369 µg/m<sup>2</sup>/s), Birmingham (TCNO<sub>2</sub> ~8.0-9.0 × 10<sup>-5</sup> moles/m<sup>2</sup>, NO<sub>x</sub> ~1.0-1.5 µg/m<sup>2</sup>/s), Leeds (TCNO<sub>2</sub>

370  $\sim 8.0\text{-}9.0 \times 10^{-5}$  moles/m<sup>2</sup>, NO<sub>x</sub>  $\sim 1.0\text{-}1.5$   $\mu\text{g}/\text{m}^2/\text{s}$ ) and Liverpool (TCNO<sub>2</sub>  $\sim 7.0\text{-}8.0 \times 10^{-5}$  moles/m<sup>2</sup>,  
371 NO<sub>x</sub>  $\sim 0.5\text{-}1.0$   $\mu\text{g}/\text{m}^2/\text{s}$ ).

372

373 To quantify the spatial relationship between the TCNO<sub>2</sub> and NO<sub>x</sub> emissions over source  
374 regions, the corresponding pixels of both data sets were sub-sampled for each UK city (79 in  
375 total), normalised by the sample mean and correlated against each other (red circles, **Figure**  
376 **4e**), which yielded a correlation  $R_{\text{city}1 \times 1} = 0.35$  (i.e. city1×1 represents 1 grid box × 1 grid box  
377 or 0.025° × 0.025° around where the city centre is located). However, as atmospheric NO<sub>2</sub> is  
378 subject to chemical reactions and meteorological processes (e.g. transport), the signal around  
379 source regions is more diluted and the peak TCNO<sub>2</sub> not necessarily centred on the source. To  
380 allow for that, the spatial resolution of the quantities over each source was degraded,  
381 averaging over 3×3 (**Figure 4f**), 5×5 (**Figure 4g**) and 7×7 (**Figure 4h**) grid cells and the  
382 correlation recalculated (e.g. city3×3 represents 3 grid boxes × 3 grid boxes or 0.075° × 0.075°  
383 around where the city centre is located). This resulted in correlations of  $R_{\text{city}3 \times 3} = 0.53$ ,  $R_{\text{city}5 \times 5}$   
384  $= 0.62$  and  $R_{\text{city}7 \times 7} = 0.52$ . The correlation for full domain (i.e. the UK) was  $R_{\text{all}} = 0.20$ . As  
385 expected, the correlation for all grid pixels (e.g. including pixels over the sea) is weak where  
386 long-range transport of NO<sub>2</sub> can yield spatial variability in background regions with  
387 corresponding zero emission pixels. The  $R_{\text{city}1 \times 1}$ ,  $R_{\text{city}3 \times 3}$ ,  $R_{\text{city}5 \times 5}$  and  $R_{\text{city}7 \times 7}$  correlations were all  
388 larger. The largest city-scale correlation was for the  $R_{\text{city}5 \times 5}$  values where the spatial variability  
389 has been smoothed and is representative of the more diffuse pattern of TCNO<sub>2</sub>. However, the  
390  $R_{\text{city}7 \times 7}$  (0.175° × 0.175° or  $\sim 15\text{-}20$  km × 15-20 km) correlation is lower than the  $R_{\text{city}5 \times 5}$  value  
391 suggesting that this scale is larger than most UK city sizes. Overall, for all R values, except for  
392  $R_{\text{all}}$ , there are statistically significant positive correlations at the 90% confidence level (CL) or  
393 above (>95% CL for  $R_{\text{city}3 \times 3}$ ,  $R_{\text{city}5 \times 5}$  and  $R_{\text{city}7 \times 7}$ ). Therefore, the city-scale emission-satellite  
394 correlations provide confidence in the spatial distribution of the NAEI NO<sub>x</sub> emissions based  
395 on the observed satellite TCNO<sub>2</sub>.

396

### 397 **3.2 Satellite NO<sub>2</sub> and Emission NO<sub>x</sub> Trends**

398

399 To evaluate the temporal evolution of the NAEI emissions, we use the long-term satellite  
400 record of TCNO<sub>2</sub> from OMI between 2005 and 2015. Annual total UK emissions of NO<sub>x</sub>  
401 (expressed as NO<sub>2</sub> here) from the NAEI start in 1970 and continue to present day (typically  
402 with a lag of approximately two years). Annual spatial maps of the NAEI also exist over the  
403 same time period. However, while there is a consistent methodology for the UK total  
404 estimates, the mapping methodology updates between years (NAEI, 2017). Therefore,  
405 instead of performing trends on the maps, we focus on trends in the UK NO<sub>x</sub> emission totals.  
406 For OMI, we have taken a similar broad scale approach focussing on averaged TCNO<sub>2</sub> across  
407 England (defined as 3°W-2°E, 50-54°N). We focus on England as the majority of large UK  
408 sources with reasonable spatiotemporal coverage are located here and have clearly defined  
409 trends over source regions. Pope et al., (2018) showed significantly (at the 95% CL) decreasing  
410 trends over London, Birmingham, Manchester and the Yorkshire power stations of between  
411 1.5% and 2.3% per year. OMI measurements can be subject to large uncertainties and  
412 variability, so this analysis also investigates trends in a range of OMI TCNO<sub>2</sub> percentiles over  
413 time. To estimate the annual absolute England total NAEI NO<sub>x</sub> emissions, we summed the  
414 emissions data for England (same geographical definition as for OMI above) from the 2019  
415 NAEI NO<sub>x</sub> emissions map and imposed the UK total NO<sub>x</sub> trend on it. Here, we use a simple  
416 linear fit which yields an annual decrease in the UK total NO<sub>x</sub> emission of 4.4%. The relative

417 rate of change is the same for the England total NO<sub>x</sub> emissions, but the absolute values are  
418 lower than the UK total NO<sub>x</sub> emissions (**Figure 5, top panel**).

419  
420 Over the 2005-2015 period, the England average OMI TCNO<sub>2</sub> trends in the 10<sup>th</sup>, 25<sup>th</sup>, 50<sup>th</sup>, 75<sup>th</sup>  
421 and 90<sup>th</sup> percentiles are  $-0.18 \times 10^{-5}$  moles/m<sup>2</sup>/yr (-3.3%/yr),  $-0.20 \times 10^{-5}$  moles/m<sup>2</sup>/yr (-  
422 2.7%/yr),  $-0.21 \times 10^{-5}$  moles/m<sup>2</sup>/yr (-2.2%/yr),  $-0.17 \times 10^{-5}$  moles/m<sup>2</sup>/yr (-1.3%/yr) and  $-0.07$   
423  $\times 10^{-5}$  moles/m<sup>2</sup>/yr (-0.4%/yr), respectively (**Figure 5**). All of the satellite trends are significant  
424 at the 95% CL except for the 90<sup>th</sup> percentile. The UK and England total NO<sub>x</sub> emission trends  
425 between 2005 and 2015 are -76.3 kt/yr and -45.5 kt/yr (both -4.4%/yr). The OMI TCNO<sub>2</sub> trends  
426 range between -3.2% and -0.4% depending on the data percentile used to generate the  
427 average England TCNO<sub>2</sub> annual time series. We also calculated annual trends in UK and  
428 England (same definition as above) surface NO<sub>2</sub> observations (**Figure 5, bottom panel**) from  
429 AURN (AURN, 2021). Here, we used urban background, suburban and rural sites. For the 10<sup>th</sup>,  
430 25<sup>th</sup>, 50<sup>th</sup>, 75<sup>th</sup> and 90<sup>th</sup> percentiles, UK (England) trends are -0.26 (-0.27) µg/m<sup>3</sup>/yr, -0.40 (-  
431 0.52) µg/m<sup>3</sup>/yr, -0.73 (-0.77) µg/m<sup>3</sup>/yr, -0.95 (-0.95) µg/m<sup>3</sup>/yr and -1.19 (-1.09) µg/m<sup>3</sup>/yr. This  
432 corresponds to -3.77 (-3.03) %/yr, -3.07 (-3.24) %/yr, -3.03 (-2.86) %/yr, -2.49 (-2.31) %/yr and  
433 -2.29 (-1.98) %/yr. Therefore, the NAEI NO<sub>x</sub> emissions trend is of similar magnitude and  
434 direction to that of the observations. The differences are most likely explained by the non-  
435 linear conversion of emissions to atmospheric concentrations (i.e. complex meteorology and  
436 chemistry). The likely drivers for decreases in UK NO<sub>x</sub> emissions and NO<sub>2</sub> concentrations  
437 include a shift to cleaner energy sources (e.g. National Emissions Ceilings Regulations 2018,  
438 DEFRA. (2018b)), regulations on industrial and power generation emissions (Environmental  
439 Permitting Regulations 2016 (UK Government, 2016)) and tighter emissions for vehicles (e.g.  
440 Euro 6 emissions standards). Overall, these results provide confidence in the use of the  
441 satellite data as a tool to evaluate bottom-up emission trends.

### 442 443 **3.3 Top-Down NO<sub>x</sub> Emissions**

444  
445 The top-down NO<sub>x</sub> emission rate for London under westerly flow (**Figure 2**) is 55.2 moles/s  
446 (357.75, 742.78 moles/s, ~~i.e. satellite total error range based on Sat NO<sub>x</sub> Emissions-1~~  
447 ~~uncertainties~~), while the NAEI flux is 30.9 moles/s. Here, the NAEI has a low bias with the top-  
448 down estimate and sits outside the uncertainty range ~~(though just sits within the Sat NO<sub>x</sub>~~  
449 ~~Emissions-2 uncertainties)~~. The top-down emissions are based on 2 years, so the flux should  
450 be representative of an annual emission rate, corresponding to the NAEI reporting. In the case  
451 of Birmingham (**Figure 3a**), under easterly flow, there is a visible plume (i.e. positive  
452 differences of  $2.0\text{-}3.0 \times 10^{-5}$  moles/m<sup>2</sup>) superimposed on a background enhancement ( $0.5\text{-}$   
453  $1.0 \times 10^{-5}$  moles/m<sup>2</sup>). As a result, the wind-flow NO<sub>2</sub> LD is always larger than the all-flow NO<sub>2</sub>  
454 LD and never reaches the background level (i.e. zero differences in **Figure 3a**) within the  
455 domain for which the TROPOMI TCNO<sub>2</sub> data has been processed for (e.g. there are positive  
456 differences in between the source, Birmingham, and the west of the domain, 8°W). Therefore,  
457 the running t-test methodology is used to determine when the wind-flow NO<sub>2</sub> LD reaches a  
458 steady background state *B*, as shown in **Figure 3b**. Overall, the NAEI (12.9 moles/s)  
459 underestimates the top-down emissions for Birmingham under easterly flow (29.0 (178.7,  
460 3940.2) moles/s).

461  
462 Our methodology was applied to 10 city sources where sources had suitable downwind TCNO<sub>2</sub>  
463 enhancements to derive NO<sub>2</sub> LDs and top-down emissions (**Figure 6**). A suitable downwind

464 TCNO<sub>2</sub> enhancement was subjectively identified when a clear TCNO<sub>2</sub> enhancement (i.e.  
465 positive anomalies) under a specific wind flow/direction occurred and a realistic lifetime (i.e.  
466 in the range of the literature – e.g. Verstraeten et al. (2018)) could be derived from the  
467 downwind TCNO<sub>2</sub> profile of the target source. These are shown in **Table 1**. Where top-down  
468 emissions could be derived for sources over several wind directions, they were averaged  
469 together. The TCNO<sub>2</sub> response to mesoscale and synoptic weather systems (i.e. large scale  
470 flow) can be seasonally influenced (e.g. Pope et al., 2015) with some wind directions occurring  
471 more frequently in certain seasons. Therefore, top-down NO<sub>x</sub> emission estimates derived  
472 from several wind directions for a particular source, though sampled throughout all months,  
473 can vary depending on the seasonal influence on the observed TCNO<sub>2</sub> for which the wind  
474 direction more frequently occurs in. The top-down emissions derived here suggest that the  
475 NAEI bottom-up emissions for the largest sources such as London, ~~Manchester~~ and  
476 Birmingham are underestimated. The top-down emissions for London, ~~Manchester~~ and  
477 Birmingham are 47.9 (31.~~27~~, 64.~~50~~) moles/s, ~~20.5 (13.0, 28.1) moles/s~~ and 22.1, (~~14~~~~13.53~~,  
478 ~~29~~~~30.98~~) moles/s with corresponding NAEI emissions of 30.9 moles, ~~10.0 moles/s~~ and 12.9  
479 moles/s, respectively. The NAEI (10.0 moles/s) also underestimates the emissions for  
480 Manchester 20.5 (3.3, 37.7) moles/s, but the top-down emission uncertainty is large  
481 (dominated by the smaller sample size of 29 days and large precision errors in the TCNO<sub>2</sub>  
482 data), so sits within its uncertainty range.

483  
484 For the smaller sources (e.g. Edinburgh, Bristol, ~~and Cardiff~~, Leeds, Norwich and Belfast), the  
485 comparisons are in better agreement with the NAEI and are located within the top-down  
486 emission ranges. However, for Newcastle the NAEI emissions (3.1 moles/s) are substantially  
487 larger than the top-down estimate (1.7 (0.~~98~~, 2.~~36~~) moles/s). ~~In contrast, for Leeds (3.4~~  
488 ~~moles/s), Norwich (1.0 moles/s and Belfast (1.6 moles), the NAEI substantially underestimates~~  
489 ~~the top-down emissions of 5.70 (3.7, 7.6) moles/s, 2.4 (1.3, 3.4) moles/s and 3.4 (2.1, 4.8)~~  
490 ~~moles/s, respectively.~~ For the NO<sub>2</sub> effective lifetime, we find it ranges between 2.9 and 7.9  
491 hours, which is consistent with values in the literature (e.g. Schaub et al., 2007; Pope et al.,  
492 2015), For all cities in **Figure 6** there is a strong correlation (0.99) between the NAEI and top-  
493 down emission sources investigated here, but the NAEI has a low bias of -4.18 moles/s (-  
494 37.4%) on average, dominated by the larger sources (i.e. London, Manchester and  
495 Birmingham). These metrics were calculated in linear space.

#### 496 497 **4. Conclusions**

498  
499 We have evaluated relationships between satellite observations (TROPOspheric Monitoring  
500 Instrument, TROPOMI) of tropospheric column nitrogen dioxide (TCNO<sub>2</sub>) and the UK National  
501 Atmospheric Emissions Inventory (NAEI) for nitrogen oxides (NO<sub>x</sub> = NO + NO<sub>2</sub>). Although they  
502 are different quantities, the short NO<sub>2</sub> lifetime means that our comparison can serve as a  
503 useful and important tool to evaluate bottom-up emissions. Here, spatial comparison of the  
504 TROPOMI TCNO<sub>2</sub> with the NAEI highlights consistency over the source regions with co-located  
505 peak values in the respective data sets. Correlation analysis of TCNO<sub>2</sub> and NO<sub>x</sub> emissions over  
506 the UK cities indicates moderate spatial agreement with R ranging between 0.4 and 0.6  
507 (significant at the >90% confidence level). Analysis of long-term satellite records of TCNO<sub>2</sub>  
508 (from the Ozone Monitoring Instrument (OMI), 2005-2015) show comparable negative trends  
509 with the NAEI NO<sub>x</sub> emissions with rates of -2.2%/yr and -4.4%/yr, respectively. Though the  
510 relative NAEI trend is larger than OMI, meteorological conditions and photochemistry will

511 control the atmospheric response to a change in NO<sub>x</sub> emissions, as seen by OMI. It is also  
512 possible that the NAEI overestimates the decreasing NO<sub>x</sub> emissions trend.

513

514 We have also used TROPOMI data to derive top-down city-scale estimates of UK NO<sub>x</sub>  
515 emissions. While it can still be challenging to derive emissions from city scale sources (e.g.  
516 frequent cloud cover in the UK), we estimate top-down emissions fluxes (using satellite data  
517 between February 2018 and January 2020) for several cities. Most of the city sources show  
518 reasonable agreement, but for larger sources like London and Birmingham, the top-down  
519 emission values are substantially larger than those in the NAEI for 2019. Overall, as far as we  
520 are aware, this study represents the first robust attempt to use satellite observations of  
521 TCNO<sub>2</sub> to evaluate and constrain the official UK bottom-up NAEI. We find spatial and temporal  
522 agreement between the two quantities, but find evidence that the NAEI NO<sub>x</sub> emissions for  
523 larger sources (e.g. London) may be too low (i.e. by >25%) sitting outside the top-down  
524 emission uncertainty ranges ~~(i.e. based on the satellite retrieval errors)~~. To fully understand  
525 the discrepancies and the drivers of these NO<sub>x</sub> emissions differences, further investigation is  
526 required.

527

528

529

530

### 531 **Data Availability**

532 TROPOMI and OMI tropospheric column NO<sub>2</sub> data comes from the Tropospheric Emissions  
533 Monitoring Internet Service (TEMIS, <https://www.temis.nl/airpollution/no2.php>). The  
534 bottom-up NO<sub>x</sub> emissions come from the National Atmospheric Emissions Inventory  
535 (<https://naei.beis.gov.uk/data/data-selector?view=air-pollutants>) and the point and area  
536 sources can be obtained from [https://naei.beis.gov.uk/data/map-uk-  
537 das?pollutant\\_id=6&emiss\\_maps\\_submit=naei-20210325121854](https://naei.beis.gov.uk/data/map-uk-das?pollutant_id=6&emiss_maps_submit=naei-20210325121854). The specific UK total NO<sub>x</sub>  
538 emissions came from <https://naei.beis.gov.uk/data/data-selector-results?q=142818>.  
539 Meteorological wind, temperature and boundary layer height data came from ECMWF  
540 ([https://cds.climate.copernicus.eu/cdsapp#!/dataset/reanalysis-era5-pressure-  
541 levels?tab=overview](https://cds.climate.copernicus.eu/cdsapp#!/dataset/reanalysis-era5-pressure-levels?tab=overview)). CAMS NO<sub>2</sub> data was retrieved from  
542 [https://ads.atmosphere.copernicus.eu/cdsapp#!/dataset/cams-global-reanalysis-  
543 eac4?tab=form](https://ads.atmosphere.copernicus.eu/cdsapp#!/dataset/cams-global-reanalysis-eac4?tab=form). The AURN data was obtained from [https://uk-  
544 air.defra.gov.uk/networks/network-info?view=aurn](https://uk-air.defra.gov.uk/networks/network-info?view=aurn).

545

### 546 **Author contribution**

547 RJP undertook the research looking at the spatial maps and long-term trends. RJP, RK, CW  
548 and AMG worked on the satellite top-down city-scale NO<sub>x</sub> emission estimates. RJP prepared  
549 the manuscript with contributions from all co-authors.

550

### 551 **Competing interests**

552 The authors declare that they have no conflict of interest.

553

### 554 **Acknowledgements**

555 This work was funded by the Department for Environment, Food and Rural Affairs  
556 Affairs through the “Applying Earth Observation (EO) to Reduce Uncertainties in Emission  
557 Inventories” project and by the UK Natural Environment Research Council (NERC) by

558 providing funding for the National Centre for Earth Observation (NCEO, award reference  
559 NE/R016518/1).

560

## 561 **References**

562 AURN. Automated Urban and Rural Network [Online]. Available: [https://uk-](https://uk-air.defra.gov.uk/networks/network-info?view=aur)  
563 [air.defra.gov.uk/networks/network-info?view=aur](https://uk-air.defra.gov.uk/networks/network-info?view=aur) (accessed 30<sup>th</sup> March 2021), 2021.

564 Beirle, S., Boersma, B.F., Platt, U., Lawrence, M.G. and Wagner, T.: Megacity emissions and  
565 lifetimes of nitrogen oxides probed from space, *Science*, 333, 1737,  
566 doi:10.1126/science.1207824, 2011.

567 Boersma, K.F., Eskes, H.J., Veefkind, J.P., Brinksma, E.J., van der A, R.J., Sneep, M., van den  
568 Oord, G.H.J., Levelt, P.F., Stammes, P., Gleason, J.F. and Bucsela, E.J.: Near-real time  
569 retrieval of tropospheric NO<sub>2</sub> from OMI, *Atmospheric Chemistry and Physics*, 7, 2103–2118,  
570 doi:10.5194/acp-7-2103-2007, 2007.

571 Braak R. 2010. Row Anomaly Flagging Rules Lookup Table, KNMI Technical Document TN-  
572 OMIE-KNMI-950, *KNMI*, Netherlands.

573 CAMS. CAMS global reanalysis (EAC4). Available:  
574 [https://ads.atmosphere.copernicus.eu/cdsapp#!/dataset/cams-global-reanalysis-](https://ads.atmosphere.copernicus.eu/cdsapp#!/dataset/cams-global-reanalysis-eac4?tab=form)  
575 [eac4?tab=form](https://ads.atmosphere.copernicus.eu/cdsapp#!/dataset/cams-global-reanalysis-eac4?tab=form) (accessed 29<sup>th</sup> November 2021), 2021.

576

577 Chan, K. L., Wiegner, M., van Geffen, J., De Smedt, I., Alberti, C., Cheng, Z., Ye, S. and Wenig,  
578 M.: MAX-DOAS measurements of tropospheric NO<sub>2</sub> and HCHO in Munich and the  
579 comparison to OMI and TROPOMI satellite observations, *Atmospheric Measurement*  
580 *Techniques*, 13, 4499–4520, doi: 10.5194/amt-13-4499-2020, 2020.

581 DEFRA. Air Pollution in the UK 2017 [Online]. Available: [https://uk-](https://uk-air.defra.gov.uk/assets/documents/annualreport/air_pollution_uk_2017_issue_1.pdf)  
582 [air.defra.gov.uk/assets/documents/annualreport/air\\_pollution\\_uk\\_2017\\_issue\\_1.pdf](https://uk-air.defra.gov.uk/assets/documents/annualreport/air_pollution_uk_2017_issue_1.pdf) (last  
583 accessed 30<sup>th</sup> March 2021), 2018a.

584 DEFRA. UK Informative Inventory Report (1990 to 2016) [Online]. Available: [https://uk-](https://uk-air.defra.gov.uk/library/reports?report_id=956)  
585 [air.defra.gov.uk/library/reports?report\\_id=956](https://uk-air.defra.gov.uk/library/reports?report_id=956) (last accessed 30<sup>th</sup> March 2021), 2018b.

586 DEFRA. Air Pollution in the UK 2019 [Online]. Available: [https://uk-](https://uk-air.defra.gov.uk/library/annualreport/viewonline?year=2019_issue_1#report_pdf)  
587 [air.defra.gov.uk/library/annualreport/viewonline?year=2019\\_issue\\_1#report\\_pdf](https://uk-air.defra.gov.uk/library/annualreport/viewonline?year=2019_issue_1#report_pdf) (accessed  
588 30<sup>th</sup> March 2021), 2020.

589 Dibbens, C. and Clemens, T.: Place of work and residential exposure to ambient air pollution  
590 and birth outcomes in Scotland, using geographically fine pollution climate mapping  
591 estimates, *Environmental Research*, 140, 535-541, doi:10.1016/j.envres.2015.05.010,  
592 (2015).

593 Dimitropoulou, E., Hendrick, F., Pinardi, G., Friedrich, M. M., Merlaud, A., Tack, F., De  
594 Loungeville, H., Fayt, C., Hermans, C., Laffineur, Q., Fierens, F. and Van Roozendael, M.:  
595 Validation of TROPOMI tropospheric NO<sub>2</sub> columns using dual-scan multi-axis differential  
596 optical absorption spectroscopy (MAX-DOAS) measurements in Uccle, Brussels, *Atmospheric*  
597 *Measurement Techniques*, 13, 5165–5191, doi: 10.5194/amt-13-5165-2020, 2020.

598 ECMWF. ERA5 hourly data on pressure levels from 1979 to present. Available at:  
599 [https://cds.climate.copernicus.eu/cdsapp#!/dataset/reanalysis-era5-pressure-](https://cds.climate.copernicus.eu/cdsapp#!/dataset/reanalysis-era5-pressure-levels?tab=overview)  
600 [levels?tab=overview](https://cds.climate.copernicus.eu/cdsapp#!/dataset/reanalysis-era5-pressure-levels?tab=overview) (accessed 29<sup>th</sup> November 2021), 2021.

601 EEA. Air quality in Europe — 2018 report [Online]. Available:  
602 <https://www.eea.europa.eu/publications/air-quality-in-europe-2018> (accessed 30<sup>th</sup> March  
603 2021), 2018.

604 EMEP/EAA. EMEP/EAA air pollutant emission inventory guidebook 2019, EEA Report No  
605 13/2019, ISSN 1977-8449. Available: [https://www.eea.europa.eu/publications/emep-eea-](https://www.eea.europa.eu/publications/emep-eea-guidebook-2019)  
606 [guidebook-2019](https://www.eea.europa.eu/publications/emep-eea-guidebook-2019) (accessed 2<sup>nd</sup> July 2021), 2019.

607

608 EMEP. EMEP – Convention on Long-range Transboundary Air Pollution. Available:  
609 <https://www.emep.int/> (accessed 12<sup>th</sup> July 2021), 2021.

610

611 Liu, F., Beirle, S., Zhang, Q., Dörner, S., He, K. and Wagner T.: NO<sub>x</sub> lifetimes and emissions of  
612 cities and power plants in polluted background estimated by satellite observations,  
613 *Atmospheric Chemistry and Physics*, 16, 5283-5298, doi:10.5194/acp-16-5283-2016, 2016.

614 Martin, R.V., Jacob, D.J., Chance, K., Kurosu, T.P., Palmer, P.I. and Evans, M.J.: Global  
615 inventory of nitrogen oxide emissions constrained by space-based observations of NO<sub>2</sub>  
616 columns, *Journal of Geophysical Research*, 108, 4537, doi:10.1029/2003JD003453, 2003.

617 Miyazaki, K., Eskes, H., Sudo, K., Boersma, K.F., Bowman, K. and Kanaya, Y.: Decadal changes  
618 in global surface NO<sub>x</sub> emissions from multi-consistent satellite data assimilation,  
619 *Atmospheric Chemistry and Physics*, 17, 807-837, doi:10.5194/acp-17-807-2017, 2016.

620 NAEI. UK Emission Mapping Methodology. – 2015 [Online]. Available: [https://uk-](https://uk-air.defra.gov.uk/assets/documents/reports/cat07/1710261436_Methodology_for_NAEI_2017.pdf)  
621 [air.defra.gov.uk/assets/documents/reports/cat07/1710261436\\_Methodology\\_for\\_NAEI\\_20](https://uk-air.defra.gov.uk/assets/documents/reports/cat07/1710261436_Methodology_for_NAEI_2017.pdf)  
622 [17.pdf](https://uk-air.defra.gov.uk/assets/documents/reports/cat07/1710261436_Methodology_for_NAEI_2017.pdf) (accessed 30<sup>th</sup> March 2021), 2017.

623 NAEI. UK-NAEI – National Atmospheric Emissions Inventory [Online]. Available:  
624 <https://naei.beis.gov.uk/> (accessed 30<sup>th</sup> March 2021), 2021.

625 Pena-Angulo, D., Reig-Gracia, F., Dominguez-Castro, F., Revuelto, J., Aguilar, E., van der  
626 Schrier, G. and Vicente-Serrano, S. M.: ECTACI: European Climatology and Trends Atlas of  
627 Climate Indices (1979-2017), *Journal of Geophysical Research: Atmospheres*, 125,  
628 e2020JD032798, doi: 10.1029/2020JD032798, 2020. Pope, R.J., Savage, N.H., Chipperfield,  
629 M.P., Ordonez, C. and Neal, L.S.: The influence of synoptic weather regimes on UK air  
630 quality: Regional model studies of tropospheric column NO<sub>2</sub>, *Atmospheric Chemistry and*  
631 *Physics*, 15, 11201-11215, doi:10.5194/acp-15-11201-2015, 2015.

632 Pope, R.J., Arnold, S.R., Chipperfield, M.P., Latter, B.G., Siddans, R. and Kerridge, B.J.:  
633 Widespread changes in UK air quality observed from space, *Atmospheric Science Letters*, 19,  
634 e817, doi: 10.1002/asl.817, 2018.

635 Potts, D.A., Marais, E.A., Boesch, H., Pope, R.J., Lee, J., Drysdale, W., Chipperfield, M.P.,  
636 Kerridge, B. and Siddans, R.: Diagnosing air quality changes in the UK during the COVID-19  
637 lockdown using TROPOMI and GEOS-Chem, *Environmental Research Letters*, 16, 054031,  
638 doi:10.1088/1748-9326/abde5d, 2021.

639 Ricardo Energy and Environment. UK Informative Inventory Report (1990 to 2019).  
640 Available: [https://uk-](https://uk-air.defra.gov.uk/assets/documents/reports/cat09/2103151107_GB_IIR_2021_FINAL.pdf)  
641 [air.defra.gov.uk/assets/documents/reports/cat09/2103151107\\_GB\\_IIR\\_2021\\_FINAL.pdf](https://uk-air.defra.gov.uk/assets/documents/reports/cat09/2103151107_GB_IIR_2021_FINAL.pdf)  
642 (accessed 2<sup>nd</sup> July 2021), 2021.

643 Royal College of Physicians. Every breath we take: the lifelong impact of air pollution  
644 [Online]. Available: [https://www.rcplondon.ac.uk/projects/outputs/every-breath-we-take-](https://www.rcplondon.ac.uk/projects/outputs/every-breath-we-take-lifelong-impact-air-pollution)  
645 [lifelong-impact-air-pollution](https://www.rcplondon.ac.uk/projects/outputs/every-breath-we-take-lifelong-impact-air-pollution) (accessed 30th March 2021), 2016.

646 Savage, N.H., Agnew, P., Davis, L.S., Ordóñez, C., Thorpe, R., Johnson, C.E., O'Connor, F.M.  
647 and Dalvi, M.: Air quality modelling using the Met Office Unified Model (AQUM OS24-26):  
648 model description and initial evaluation, *Geoscientific Model Development*, 6, 353–372,  
649 doi:10.5194/gmd-6-353-2013, 2013.

650 Schaub, D., Brunner, D., Boersma, K.F., Keller, J., Folini, D., Buchmann, B., Berresheim, H.  
651 and Staehelin, J.: SCIAMACHY tropospheric NO<sub>2</sub> over Switzerland: estimates of NO<sub>x</sub> lifetime  
652 and impacts of the complex alpine topography on the retrieval, *Atmospheric Chemistry and*  
653 *Physics*, 7, 5971-5987, doi:10.5194/acp-7-5971-2007, 2007.

654 Seinfeld, J. and Pandis, S.: Atmospheric Chemistry and Physics: From Air Pollution to Climate  
655 Change - Second Edition, John Wiley and Sons Inc, New Jersey, USA, 2006.

656 Torres, O., Bhartia, P. K., Jethva, H. and Ahn, C.: Impact of the ozone monitoring instrument  
657 row anomaly on the long-term record of aerosol products, *Atmospheric Measurement*  
658 *Techniques*, 11, 2701-2715, doi:10.5194/amt-11-2701-2018, 2018.

659 Tsagatakis, I., Richardson, J., Evangelides, C., Pizzolato, M., Pearson, B., Passant, N.,  
660 Pommier, M. and Otto, A.: UK Spatial Emissions Methodology: A report of the National  
661 Atmospheric Emission Inventory 2019. Available at: [https://uk-](https://uk-air.defra.gov.uk/assets/documents/reports/cat09/2107291052_UK_Spatial_Emissions_Methodology_for_NAEI_2019_v1.pdf)  
662 [air.defra.gov.uk/assets/documents/reports/cat09/2107291052\\_UK\\_Spatial\\_Emissions\\_Met](https://uk-air.defra.gov.uk/assets/documents/reports/cat09/2107291052_UK_Spatial_Emissions_Methodology_for_NAEI_2019_v1.pdf)  
663 [hodology\\_for\\_NAEI\\_2019\\_v1.pdf](https://uk-air.defra.gov.uk/assets/documents/reports/cat09/2107291052_UK_Spatial_Emissions_Methodology_for_NAEI_2019_v1.pdf) (accessed 29th November 2021), 2021.

664 UK Government. The Environmental Permitting (England and Wales) Regulations 2016.  
665 Available: <https://www.legislation.gov.uk/uksi/2016/1154/contents/made> (last accessed 2<sup>nd</sup>  
666 July 2021), 2016.

667 Veefkind, J.P., Aben, I., McMullan, K., Forster, H., de Vries, J., Otter, G., Claas, J., Eskes, H.J.,  
668 de Haan, F., Kleipool, Q., van Weele, M., Hasekamp, O., Hoogeveen, R., Landgraf, J., Snel, R.,  
669 Tol, P., Ingmann, P., Voors, R., Kruizinga, B., Vink, R., Visser, H. and Levelt, P.F.: TROPOMI on  
670 the ESA Sentinel-5 Precursor: A GMES mission for global observations of atmospheric  
671 composition for climate, air quality and ozone layer applications, *Remote Sensing of*  
672 *Environment*, 120, 70-83, doi:10.1016/j.rse.2011.09.027, 2012.

673 Verhoelst, T., Compernelle, S., Pinaridi, G., Lambert, J. C., Eskes, H., Eichmann, K. U., et al.:  
674 Ground-based validation of the Copernicus Sentinel-5P TROPOMI NO<sub>2</sub> measurements with  
675 the NDACC ZSL-DOAS, MAX-DOAS and Pandonia global networks, *Atmospheric*  
676 *Measurement Techniques*, 14, 481–510, doi: 10.5194/amt-14-481-2021, 2021.

677 Verstraeten, W.W., Boersma, K.F., Douros, J., Williams, J.E., Eskes, H., Liu, F., Beirle, S. and  
678 Delcloo, A.: Top-down NO<sub>x</sub> emissions of European cities based on the downwind plume of  
679 modelled and space-borne tropospheric NO<sub>2</sub> column, *Sensors*, 18 (9), 2893,  
680 doi:10.3390/s18092893, 2018.

681 WHO. Ambient (outdoor) air pollution [Online]. Available: [https://www.who.int/news-](https://www.who.int/news-room/fact-sheets/detail/ambient-(outdoor)-air-quality-and-health)  
682 [room/fact-sheets/detail/ambient-\(outdoor\)-air-quality-and-health](https://www.who.int/news-room/fact-sheets/detail/ambient-(outdoor)-air-quality-and-health) (last accessed 30<sup>th</sup> March  
683 2021), 2018.

684 Wu, H., Reis, S., Lin, C. and Heal, M.R.: Effect of monitoring network design on land use  
685 regression models for estimating residential NO<sub>2</sub> concentration, *Atmospheric Environment*,  
686 149, 24-33, doi:10.1016/j.atmosenv.2016.11.014, 2017.

687

688

689

690

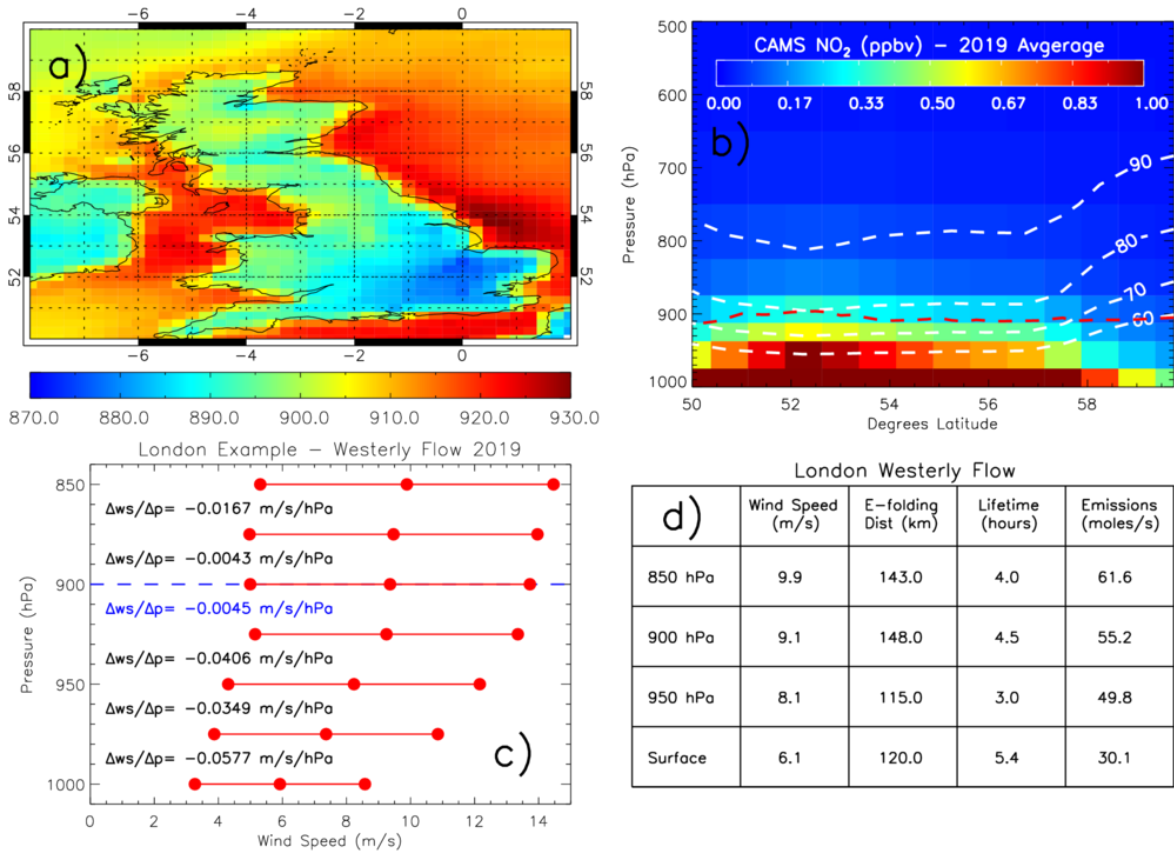
691

692

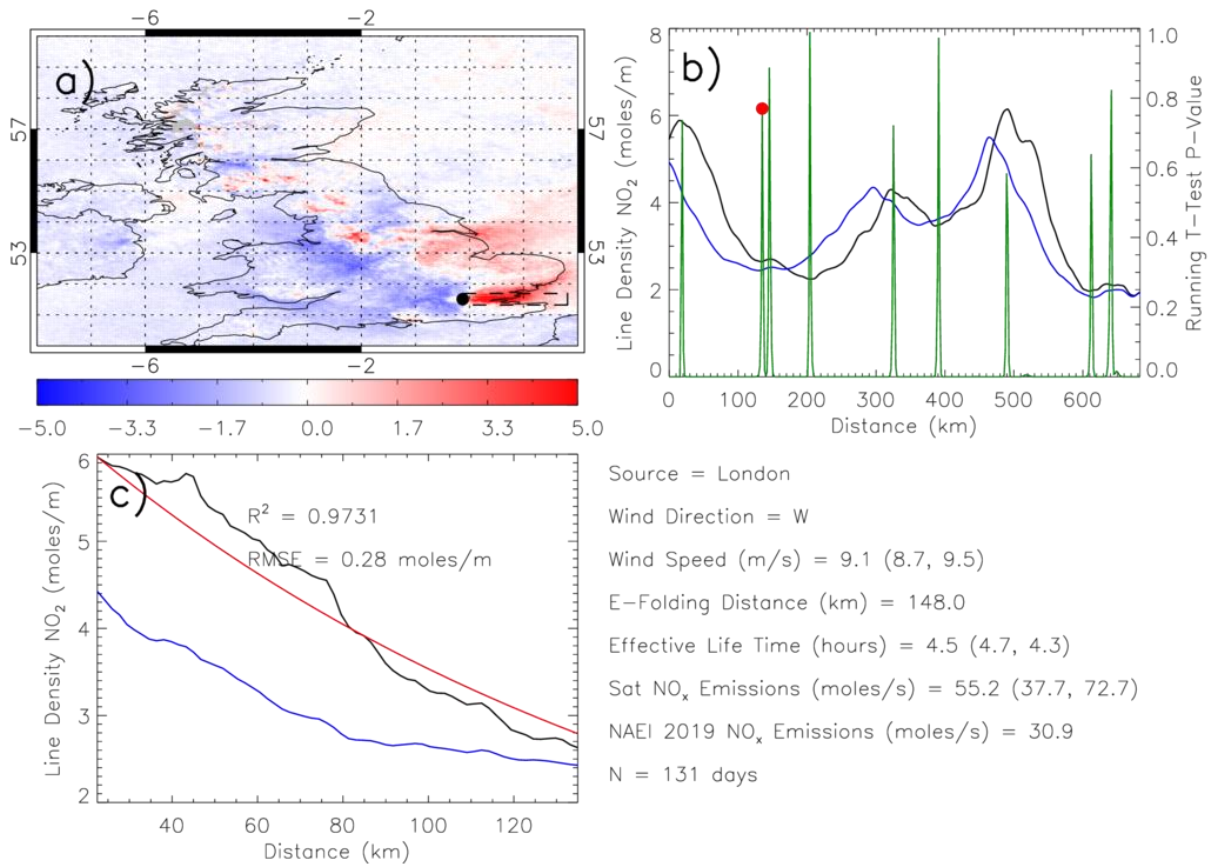
693

694

695 **Figures**

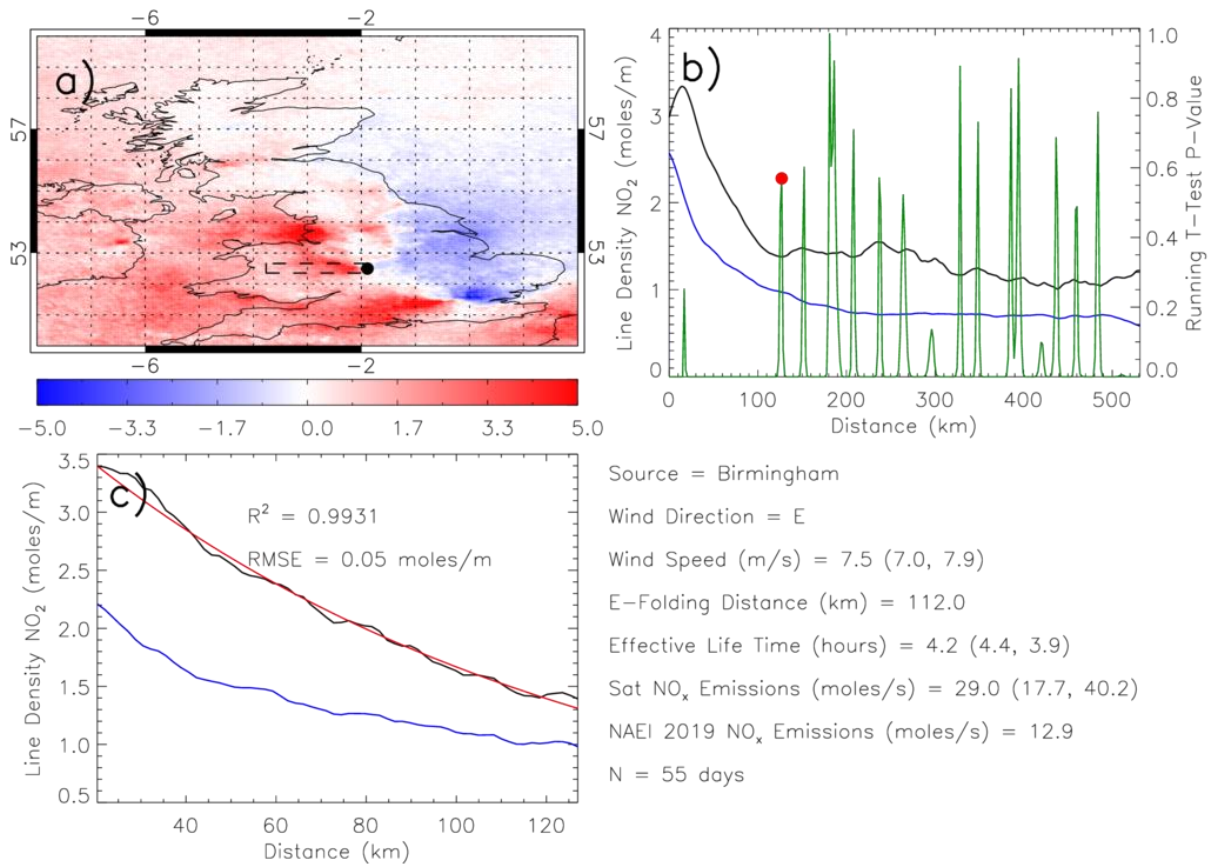


696  
 697 **Figure 1:** a) ERA-5 UK boundary layer pressure (hPa) sampled at 13.00 LT (to coincide with  
 698 the TROPOMI overpass time) and averaged for 2019. b) CAMS reanalysis zonal (8.0°W-2.0°E)  
 699 average latitude-pressure NO<sub>2</sub> (ppbv) cross-section over the UK between the surface and 500  
 700 hPa. White dashed lines represent the percentage of the surface-500 hPa NO<sub>2</sub> loading  
 701 between the surface and the respective pressure levels. The red dashed line represents the  
 702 zonal average boundary layer pressure (hPa). c) Average (surface to pressure level) wind  
 703 speed (m/s),  $\pm$  the standard deviation, profile over London under westerly flow (determined  
 704 from the ERA-5 u-wind and v-wind components at each pressure level).  $\Delta w_s/\Delta p$  is the wind  
 705 speed gradient between pressure levels. The blue text indicates the first small step change in  
 706 the gradient indicative of reduced flow turbulence and a suitable surface-altitude range to  
 707 average the winds speeds over. d) The table shows the impact to the NO<sub>x</sub> emission  
 708 parameters when using different altitudes over which to average the wind speeds.  
 709



710

711 **Figure 2:** (a) TROPOMI TCNO<sub>2</sub> ( $10^{-5}$  moles/m<sup>2</sup>) sub-sampled under westerly flow (defined  
 712 over London, black dot) minus the long-term average (February 2018 to January 2020). The  
 713 dashed box represents the width of the source and distance between the source and  
 714 background. (b) Downwind NO<sub>2</sub> LD from London (black = westerly flow, blue = all-flow  
 715 average) with the corresponding running t-test p-value (green line). The red dot represents  
 716 the location of background level determined by the turning point in the running t-test p-  
 717 value time series. (c) The westerly flow and all-flow NO<sub>2</sub> LD between peak westerly flow NO<sub>2</sub>  
 718 LD and the background value. The red line represents the e-folding distance fit with the  
 719 corresponding R<sup>2</sup> and root mean square error (RMSE) between the westerly flow NO<sub>2</sub> LD and  
 720 fit profile. N represents the number of days classified under westerly flow over London.  
 721

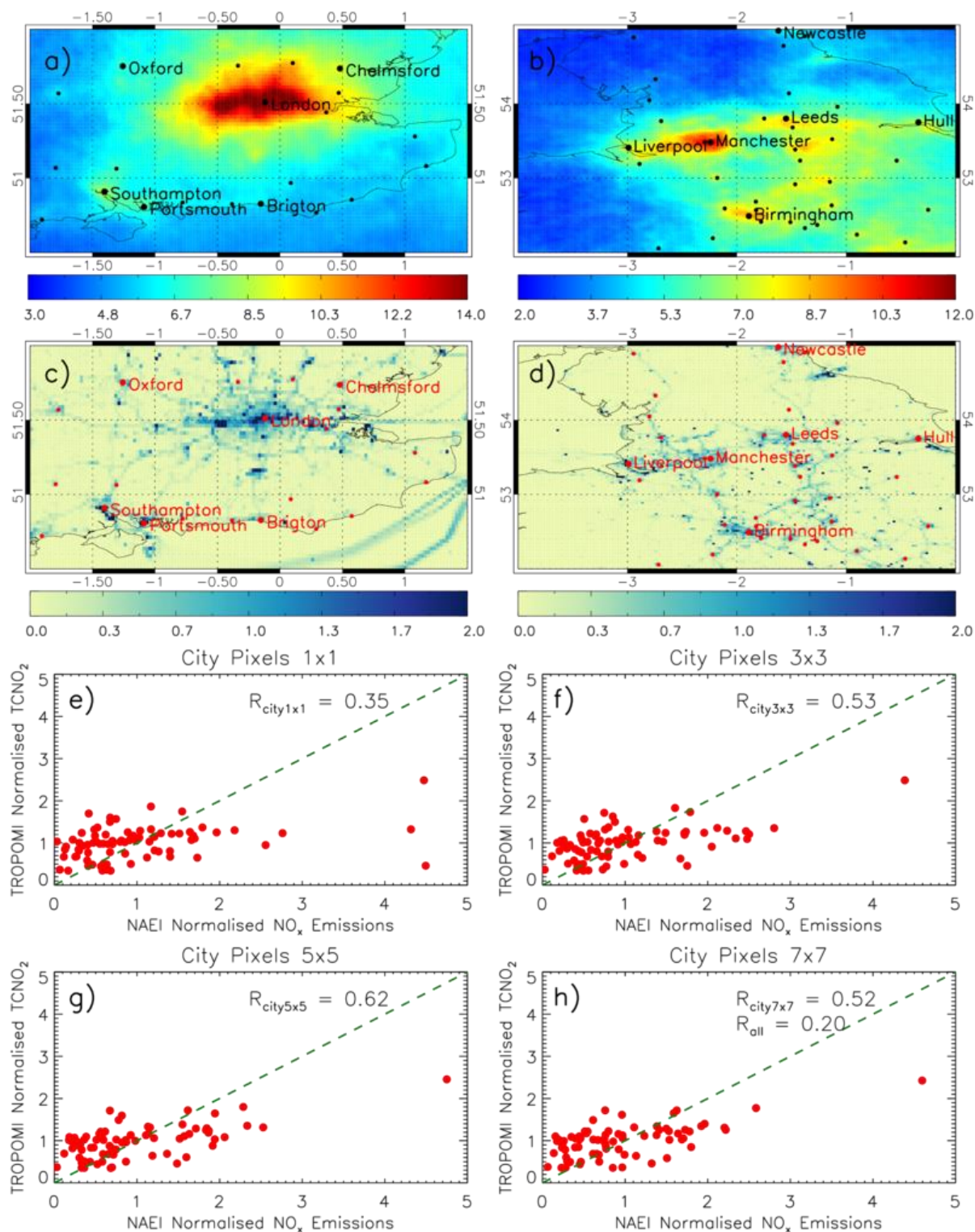


722

723 **Figure 3:** (a) TROPOMI TCNO<sub>2</sub> ( $10^{-5}$  moles/m<sup>2</sup>) sub-sampled under easterly flow (defined over  
 724 Birmingham, black dot) minus the long-term average (February 2018 to January 2020). The  
 725 dashed box represents the width of the source and distance between the source and  
 726 background. (b) Downwind NO<sub>2</sub> LD from Birmingham (black = easterly flow, blue = all-flow  
 727 average) with the corresponding running t-test p-value (green line). The red dot represents  
 728 the location of background level determined by the turning point in the running t-test p-  
 729 value time series. (c) The easterly flow and all-flow NO<sub>2</sub> LD between peak easterly flow NO<sub>2</sub>  
 730 LD and the background value. The red line represents the e-folding distance fit with the  
 731 corresponding R<sup>2</sup> and root mean square error (RMSE) between the easterly flow NO<sub>2</sub> LD and  
 732 fit profiles. N represents the number of days classified under easterly flow over Birmingham.

733

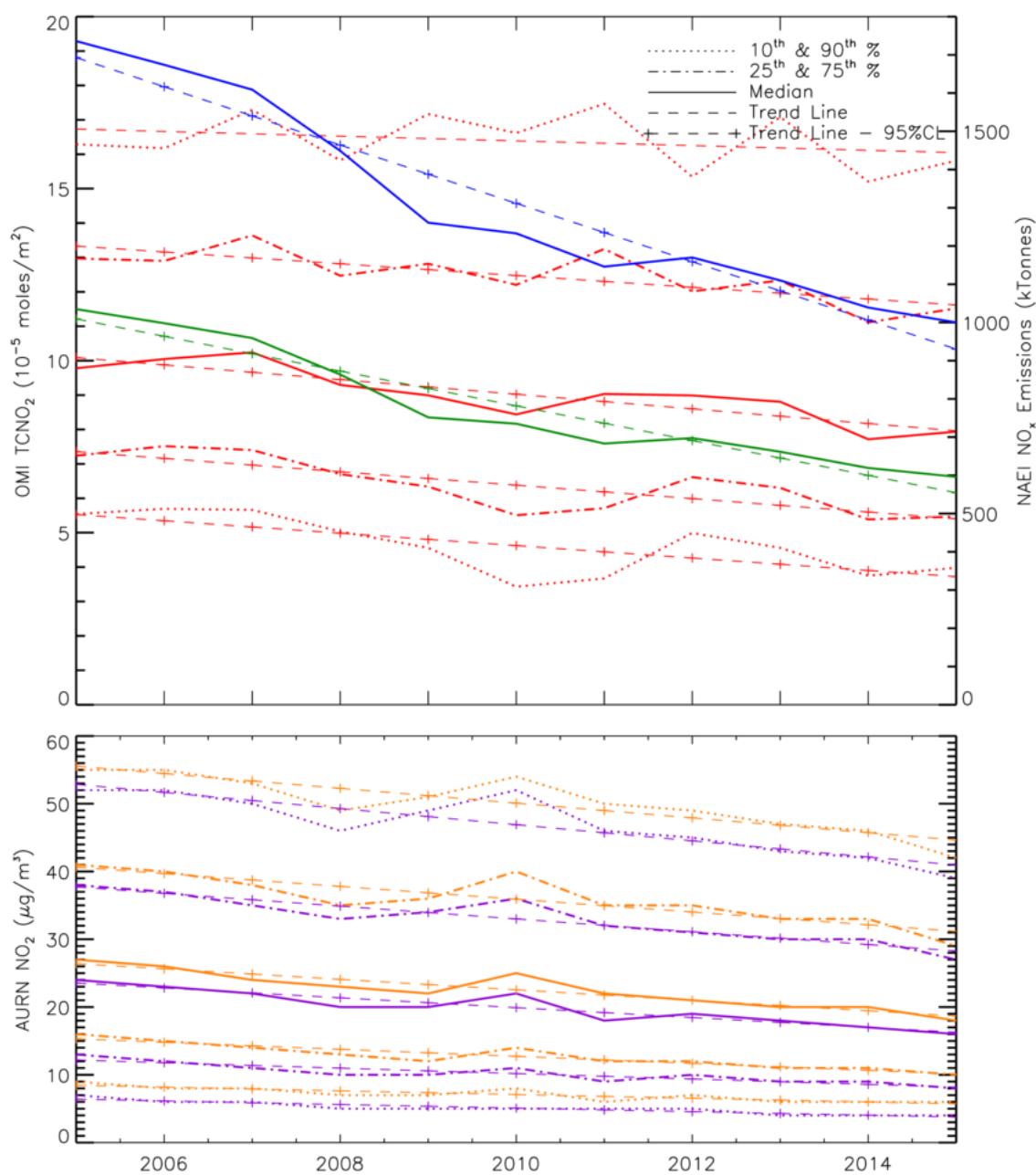
734



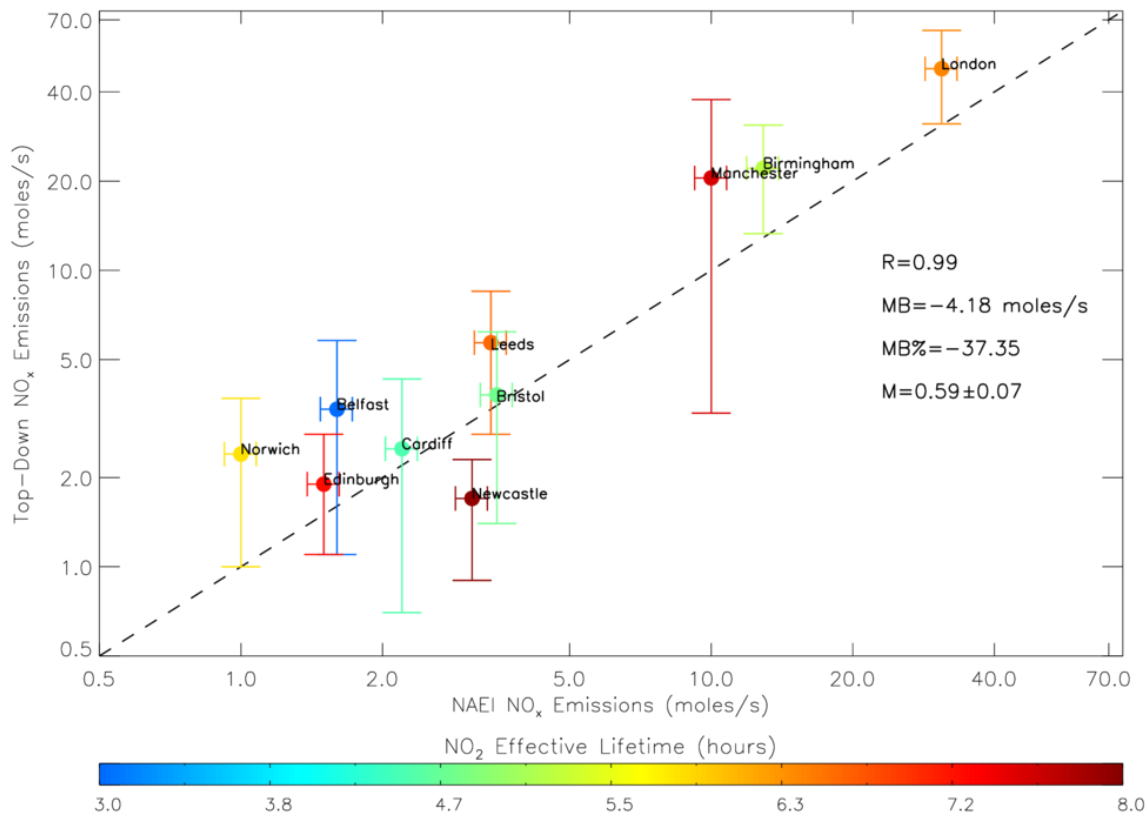
736

737 **Figure 4:** TROPOMI TCNO<sub>2</sub> ( $\times 10^{-5}$  moles/m<sup>2</sup>) average for February 2018 to January 2020  
 738 across (a) south-eastern and (b) northern England. Black circles represent city locations. NAEI  
 739 NO<sub>x</sub> emissions ( $\mu\text{g}/\text{m}^2/\text{s}$ ) for 2019 across (c) south-eastern and (d) northern England. Red  
 740 circles represent city locations. Panels (e)-(h) represent the correlation of normalised TCNO<sub>2</sub>  
 741 and NO<sub>x</sub> emissions for UK cities. The green dashed line is the 1:1 line. Each source is  
 742 normalised by the average of all the sources. The four panels also represent city means using

743 *varying pixel ranges around the source (i.e. 1×1, 3×3, 5×5 and 7×7 grid pixels). The*  
744 *correlations between the city-scale normalised NO<sub>x</sub> emissions and TCNO<sub>2</sub> are shown (R).*  
745



746  
 747 **Figure 5:** The top panel shows time series (2005 to 2015) in OMI TCNO<sub>2</sub> ( $\times 10^{-5}$  moles/m<sup>2</sup>) and  
 748 NAEI NO<sub>x</sub> emission totals (kt or Gg). OMI median, 10<sup>th</sup> & 90<sup>th</sup> and 25<sup>th</sup> & 75<sup>th</sup> percentiles are  
 749 represented by solid, dotted and dot-dashed lines, respectively. NAEI NO<sub>x</sub> emission totals for  
 750 the UK and England are represented by the blue and green solid lines. Here, the OMI TCNO<sub>2</sub>  
 751 has been averaged over England (defined as 3°W-2°E, 50-54°N) and while the UK NO<sub>x</sub> emission  
 752 totals are directly reported by the NAEI, the England NO<sub>x</sub> emission totals have been summed  
 753 over the emissions maps for the same England definition used for OMI (see Section 3.2 for  
 754 more information). In the bottom panel, AURN surface NO<sub>2</sub> ( $\mu\text{g}/\text{m}^3$ ) times series are shown  
 755 for the UK (purple) and England (orange). Trends lines are shown by dashed and dash-crossed  
 756 lines for insignificant and significant trends (at the 95% confidence level).  
 757



758

759 **Figure 6:** NAEI and top-down (TROPOMI) NO<sub>x</sub> emissions (moles/s) for 10 UK cities coloured  
 760 by the NO<sub>2</sub> effective lifetime (hours). Where there is more than one top-down estimate for a  
 761 city from multiple wind directions, the corresponding emission rates and lifetimes have been  
 762 averaged together. The correlation ( $R$ ), mean bias ( $MB$ , moles/s, *i.e.* NAEI-top down),  
 763 percentage mean bias ( $MB\%$ )-and linear fit ( $M$ , *i.e.* top down vs. NAEI) are also shown. NAEI  
 764 uncertainty is  $\pm 7.8\%$  (DEFRA, 2018b) and the top-down uncertainty range is based on  
 765 satellite errors (*i.e.* Sat Emissions 1, see text). The black dashed line represents the 1:1  
 766 relationship and both axes are on log scales.

767

768

769

770

771

772

773

774

775

776

777

778

779

780

781

782

783

784  
785  
786  
787  
788  
789

**Table 1:** List of top-down NO<sub>x</sub> (moles/s) emission estimates for UK city sources under different wind directions. The Sat NO<sub>x</sub> Emissions lower and upper ranges -1- represents the emission flux ± the total error, estimated using the TROPOMI NO<sub>2</sub> ± the retrieval uncertainty, while Sat NO<sub>x</sub> Emissions -2 is based on the lifetime derived from the wind speed data ± 1.0 sigma standard deviation.

Source Name	London	London	London	Birmingham
Longitude	-0.13	-0.13	-0.13	-1.89
Latitude	51.51	51.51	51.51	52.50
Lon Edge - West	-0.52	-0.52	-0.52	-2.18
Lon Edge - East	0.28	0.28	0.28	-1.72
Lat Edge - South	51.32	51.32	51.32	52.35
Lat Edge - North	51.69	51.69	51.69	52.66
Wind Speed Average (m/s)	9.10	7.00	7.50	7.50
Wind Speed Standard <u>Error</u> (m/s)	<u>4.300.40</u>	<u>3.200.50</u>	<u>3.100.40</u>	<u>3.200.50</u>
Wind Direction	W	N	E	E
E-Folding Distance (km)	148.00	189.00	195.00	112.00
Life Time (hr)	4.50	7.50	7.20	4.20
Life Time- Lower Wind (hr)	<u>8.604.70</u>	<u>13.808.10</u>	<u>12.407.60</u>	<u>7.304.40</u>
Life Time- Upper Wind (hr)	<u>3.104.30</u>	<u>5.207.10</u>	<u>5.106.80</u>	<u>2.903.90</u>
Satellite Emission Rate (moles/s)	55.20	55.90	32.50	29.00
Sat NO <sub>x</sub> Emissions-1 - Lower (moles/s)	<u>35.3.950</u>	<u>37.4033.9</u>	22.0±0	178.70
Sat NO <sub>x</sub> Emissions-1 - Upper (moles/s)	<u>72.74.80</u>	<u>74.3077.8</u>	42.980	<u>4039.20</u>
<u>Sat NO<sub>x</sub> Emissions-2 - Lower (moles/s)</u>	<u>29.00</u>	<u>30.50</u>	<u>18.80</u>	<u>16.40</u>
<u>Sat NO<sub>x</sub> Emissions-2 - Upper (moles/s)</u>	<u>81.30</u>	<u>81.20</u>	<u>46.10</u>	<u>41.50</u>
NAEI Emission Rate (moles/s)	30.90	30.90	30.90	12.90
<u>Number of Days</u>	<u>131</u>	<u>53</u>	<u>54</u>	<u>55</u>

790

Source Name	Birmingham	Birmingham	Newcastle	Manchester
Longitude	-1.89	-1.89	-1.62	-2.25
Latitude	52.50	52.50	54.98	53.50
Lon Edge - West	-2.18	-2.18	-1.73	-2.47
Lon Edge - East	-1.72	-1.72	-1.40	-2.01
Lat Edge - South	52.35	52.35	54.92	53.37
Lat Edge - North	52.66	52.66	55.02	53.60
Wind Speed Average (m/s)	5.80	9.10	10.50	5.60
Wind Speed Standard <u>Error</u> (m/s)	<u>2.600.30</u>	<u>4.700.40</u>	<u>4.300.30</u>	<u>2.500.40</u>
Wind Direction	N	S	W	N
E-Folding Distance (km)	184.00	91.00	297.00	152.00
Life Time (hr)	8.70	2.80	7.90	7.50
Life Time- Lower Wind (hr)	<u>15.809.40</u>	<u>5.802.90</u>	<u>13.608.10</u>	<u>13.608.20</u>
Life Time- Upper Wind (hr)	<u>6.008.20</u>	<u>1.802.60</u>	<u>5.607.60</u>	<u>5.206.90</u>
Satellite Emission Rate (moles/s)	12.20	25.20	1.70	20.5
Sat NO <sub>x</sub> Emissions-1 - Lower (moles/s)	<u>85.810</u>	16.570	0.980	<u>3.3013.00</u>
Sat NO <sub>x</sub> Emissions-1 - Upper (moles/s)	<u>16.4018.70</u>	33.970	2.630	<u>28.1037.7</u>
<u>Sat NO<sub>x</sub> Emissions-2 - Lower (moles/s)</u>	<u>6.80</u>	<u>12.20</u>	<u>1.00</u>	<u>11.30</u>

<del>Sat NOx Emissions-2 – Upper (moles/s)</del>	<del>17.70</del>	<del>38.20</del>	<del>2.40</del>	<del>29.80</del>
NAEI Emission Rate (moles/s)	12.90	12.90	3.10	10.00
<u>Number of Days</u>	<u>46</u>	<u>100</u>	<u>157</u>	<u>29</u>

791

Source Name	Belfast	Edinburgh	Norwich	Cardiff
Longitude	-5.93	-3.19	1.29	-3.18
Latitude	54.61	55.96	52.63	51.49
Lon Edge - West	-6.00	-3.32	1.20	-3.36
Lon Edge - East	-5.84	-3.10	1.38	-3.10
Lat Edge - South	54.55	55.89	52.60	51.45
Lat Edge - North	54.70	55.98	52.69	51.55
Wind Speed Average (m/s)	8.30	10.10	10.30	5.30
Wind Speed Standard <u>Error</u> (m/s)	<u>4-100.60</u>	<u>4-200.30</u>	<u>4-80.40</u>	<u>2-500.40</u>
Wind Direction	E	W	W	N
E-Folding Distance (km)	87.00	262.00	214.00	86.00
Life Time (hr)	2.90	7.20	5.80	4.50
Life Time- Lower Wind (hr)	<u>5-803.10</u>	<u>12-207.40</u>	<u>11-006.10</u>	<u>8-604.90</u>
Life Time- Upper Wind (hr)	<u>1-902.70</u>	<u>5-107.0</u>	<u>3-905.60</u>	<u>3-004.20</u>
Satellite Emission Rate (moles/s)	3.40	1.90	2.40	2.50
Sat NOx Emissions-1 - Lower (moles/s)	<u>12.10</u>	<u>01.180</u>	<u>1.030</u>	<u>1-500.70</u>
Sat NOx Emissions-1 - Upper (moles/s)	<u>54.80</u>	<u>23.810</u>	<u>3.470</u>	<u>3-504.30</u>
<del>Sat NOx Emissions-2 – Lower (moles/s)</del>	<del>1.70</del>	<del>1.10</del>	<del>1.20</del>	<del>1.30</del>
<del>Sat NOx Emissions-2 – Upper (moles/s)</del>	<del>5-20</del>	<del>2-70</del>	<del>3-50</del>	<del>3-70</del>
NAEI Emission Rate (moles/s)	1.60	1.50	1.00	2.20
<u>Number of Days</u>	<u>47</u>	<u>187</u>	<u>122</u>	<u>37</u>

792

Source Name	Leeds	Bristol
Longitude	-1.55	-2.59
Latitude	53.80	51.46
Lon Edge - West	-1.69	-2.74
Lon Edge - East	-1.44	-2.47
Lat Edge - South	53.74	51.40
Lat Edge - North	53.86	51.55
Wind Speed Average (m/s)	8.70	7.20
Wind Speed Standard <u>Error</u> (m/s)	<u>4-500.50</u>	<u>3-400.40</u>
Wind Direction	S	E
E-Folding Distance (km)	207.00	123.00
Life Time (hr)	6.60	4.70
Life Time- Lower Wind (hr)	<u>13-907.00</u>	<u>8-905.10</u>
Life Time- Upper Wind (hr)	<u>4-306.30</u>	<u>3-204.50</u>
Satellite Emission Rate (moles/s)	5.70	3.80
Sat NOx Emissions-1 - Lower (moles/s)	<u>3-702.80</u>	<u>2-501.40</u>
Sat NOx Emissions-1 - Upper (moles/s)	<u>7-608.50</u>	<u>5-106.20</u>
<del>Sat NOx Emissions-2 – Lower (moles/s)</del>	<del>2.70</del>	<del>2.00</del>
<del>Sat NOx Emissions-2 – Upper (moles/s)</del>	<del>8.60</del>	<del>5.50</del>
NAEI Emission Rate (moles/s)	3.40	3.50

793  
794

<u>Number of Days</u>	<u>81</u>	<u>55</u>
-----------------------	-----------	-----------